

PIR/corrector+Echidna Engineering Summary

Masayuki Akiyama (Astronomical Institute, Tohoku University)

- Ver.5.0 : 2008/11/13 : Updated with 2008/10 engineering results (200805eng/200810eng.tex).
- Ver.4.0 : 2008/09/10 : Updated with 2008/09 engineering results (200805eng/200809eng.tex).
- Ver.3.0 : 2008/09/04 : Updated with 2008/08 engineering results (200805eng/200808eng.tex)
- Ver.2.1 : 2008/08/11 : Bug fixed.
- Ver.2.0 : 2008/08/10 : Updated with 2008/06 engineering results (200805eng/200806eng.tex)
- Ver.1.0 : 2008/06/05 : Updated 2007/12 report with 2008/01,2008/05 engineering results (200805eng/200805eng.tex)
- Ver.-1.1 : 2008/01/18 : Bug fixed, the FPI coordinate of the distortion center is updated to be (2.4mm, 4.0mm) after applying the SKY and SPINE camera offset (positioner/ECH_test/200801eng.tex). Updated result is consistent with the offset between the CMM center and the rotator axis. The target was M38 (not M37).
- Ver.-1.0 : 2008/01/17 : Previous report circulated AAO/Kyoto/Subaru.

This is a summary of the Echidna engineering observations for the telescope model construction.

1 Converting the SKY CCD coordinate to the FPI XY coordinate

The relation between the SKY camera coordinate and the FPI XY coordinates is determined by taking stars with moving SKY camera in FPI X and Y directions. The determined relation between CCD camera coordinate (local) and the FPI XY coordinate (global) is described with

$$\begin{aligned} X(\text{FPI}) &= A \times X(\text{CCD}) + B \times Y(\text{CCD}) + C + \text{FPI}_x, \\ Y(\text{FPI}) &= D \times X(\text{CCD}) + E \times Y(\text{CCD}) + F + \text{FPI}_y \\ C &= X \text{ correction for the offset between the SKY and SPINE cameras} \\ F &= Y \text{ correction for the offset between the SKY and SPINE cameras} \end{aligned} \tag{1}$$

(We use the SKY coordinate definition measured on the FITS images, i.e. (0,0) at the bottom left of the images.)

The XY offset between SKY and SPINE cameras are determined by aligning a guide fibre to a bright star. Two measurements were performed with the same guide fiber to different stars. There results are shown as parameters C and F in Table 1. Using these values as the offset

Date	A	B	C	D	E	F	Note
200712	-8.103	+0.677	+3445	-0.668	-8.268	+2876	175.3deg rotation
200712			+3556			+2821	
Sky-camera reinstall							
200805	-8.082	-0.251	+3556	+0.388	-8.673	+2641	
200805			+3550			+2639	
Sky-camera reinstall							
200807							
200808	-8.041	+0.203	+3575	-0.195	-8.364	+2610	Current value

Table 1: The measured sky-camera to FPI coordinate conversion factors.

Date	EL	Note	
20071208	~80	(-702, -727)	
Echidna reinstall			
20080125	85	(-826, -712)	
20080125	27	(-826, -712) No significant shift from El=85deg.	
Echidna reinstall			
20080513	~80	(-754, -567)	
20080617	~80	(-739, -577) This value used for 200806 data	
20080617		(-666, -597)	
Echidna reinstall			
20080814	~80	(-699, -645)	
FAM tilt adjusted			
20080910	~80	(-459, -531)	
20081010	~40	(-456, -521) Current value	

Table 2: The measured FPI coordinates of the rotator axis. The shifts of the FPI coordinates reflect the shift of the Echidna against the rotator axis. After the FAM tilt adjustment, the rotator center changed significantly although the Echidna was not reinstalled.

between the SKY and SPINE cameras in relation (1), the coordinates measured with the SKY camera can be converted to the spine positions measured with the SPINE camera. (In order to align a star to guide spine No.168, we need to move telescope by $+878.48''$, $-243.09''$ (or $+901.76''$, $-258.28''$).

The FPI XY directions and the celestial coordinates NE directions are aligned well. The relation is summarized in Figure 1.

2 Rotator axis on the FPI coordinate

The axis of the rotator is measured by taking stars with the sky-camera with rotating the instrument. The measured CCD coordinate were converted to FPI coordinate using the relation (1). On 20080125, the rotation axis was measured at EL=85deg and at EL=27deg (At EL=27deg, the position of the FPI was kept at (0,0) referring the FPI encoder values, otherwise the recorded star track is not on a circle due to the flexure of the FPI gantry. The movement of the FPI was $\pm 200\mu\text{m}$ at most at EL=27deg). No shift was observed. The difference of the FPI

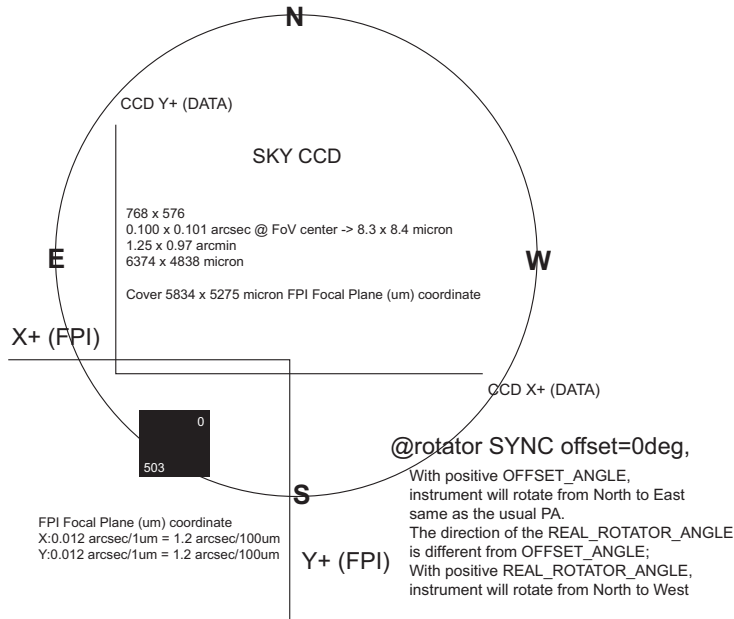


Figure 1: The relation between the sky camera CCD coordinate, the FPI XY coordinate, and the celestial coordinate. It should be noted that the SKY camera Y coordinate is flipped on the data and the Echidna GUI window.

coordinate of the pointing center between 20071208 and 20080125 measurements is $(-124, +15)$ (in μm), which represents the accuracy of the installation of Echidna unit to PIR enclosure (we remove Echidna 20080110 and re-install 20080117, it should be noted that this is not related to the accuracy of the PIR mounting accuracy).

3 Measuring the movement of the center of the distortion pattern (1)

We observed open cluster fields with tiling the SKY camera FoVs in vertical and horizontal strips on the FPI coordinate. The data are taken with the instrument rotator with SYNC status, i.e. the instrument is rotated against the corrector - primary mirror system. The measured coordinates of the stars on the SKY camera were at first converted to the FPI XY coordinate using the above relation. Then the FPI XY catalog was cross matched with the RA-DEC catalog of the stars in the FoVs. Using the (X, Y, RA, DEC) file, the distortion pattern of the field is determined by ccmmap command in IRAF. One measurement of the distortion pattern is shown in Figure 2. The offset from the plate scale at the center of FoV is shown as the optical distortion pattern. The distortions are determined by ccmmap command in IRAF. The measured distortion is consistent with the ray trace result shown with green lines and dots. The FPI XY coordinate of the distortion center was estimated to be $(-4.6\text{mm}, -1.9\text{mm})$ for this measurement.

In the nights of 20080124 and 20080125, the same measurements are done with changing the rotator angle. The results are summarized in Table 1 and Figure 3. The center of the circle of the distortion pattern movement is consistent with the rotator axis described in Section 2.

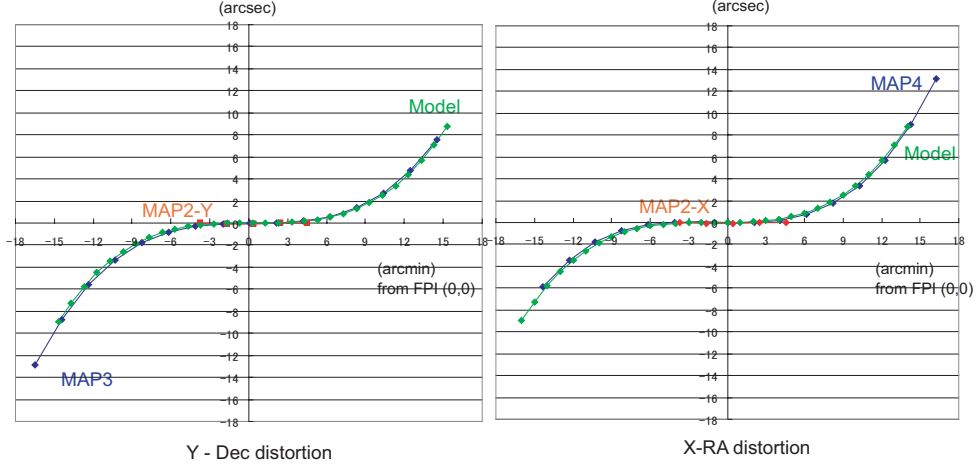


Figure 2: The measured distortion of the corrector lens in 20071224 with rotator angle of -97deg . Horizontal axis is the distance from the FPI (0,0) position in arcmin. Vertical axis is the offset from the 0.01240 (or 0.01237) arcsec/ μm in arcsec. Left) in Y (or Dec) direction, MAP2-Y and MAP3 results are shown in red and blue, respectively. Ray trace model is shown in green. The model is offsetted by -0.39arcmin (-1.9mm) to match the observed distortion curve. Right) in X (or RA) direction, MAP2-X and MAP4 results are shown in red and blue, respectively. Ray trace model is shown in green. The model is offsetted by -0.95 arcmin (-4.6mm).

Date	EL	Rotator	CMM(mm)	FAM	Distortion Cnt. (μm)	Scale ($''/\text{mm}$)
20071224	45	-97	(+4.0, -4.0)	+0.60	($-4600, -1940$)	(12.398, 12.401)
20080124	30	+0	(+3.7, -3.8)	+0.55	(+980, -4630)	(12.405, 12.409)
	30	-90	(+3.7, -3.8)	+0.55	($-4540, -2720$)	(12.411, 12.401)
	30	+90	(+3.7, -3.8)	+0.55	(+3180, +970)	(12.409, 12.401)
	30	+180	(+3.7, -3.8)	+0.55	($-2740, +3260$)	(12.420, 12.416)
20080125	85	+6	(+3.7, -3.8)	+0.60	(+1680, -4260)	(12.405, 12.405)
	85	-84	(+3.7, -3.8)	+0.60	($-4670, -3720$)	(12.400, 12.403)
	85	-174	(+3.7, -3.8)	+0.60	($-3350, +3130$)	(12.404, 12.402)
	85	+96	(+3.7, -3.8)	+0.60	(+3000, +1650)	(12.404, 12.408)
20080513			(+4.7, -4.2)	-5.00		

Table 3: Summary of the results of the distortion center measurements.

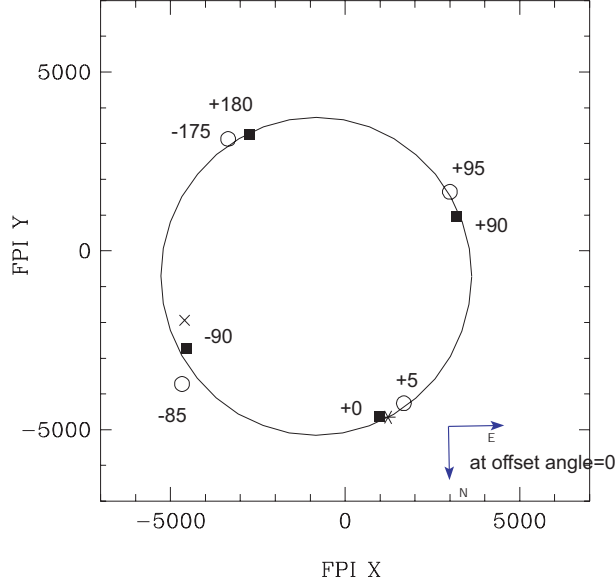


Figure 3: The measured positions of the distortion pattern center on the FPI coordinate from 200801 engineering observations. The numbers in the figure indicate the ROTATOR_REAL_ANGLE during the measurements. The measured distortion centers locate on a circle around the rotator center with radius of 4.444mm (shown with the large circle). The asterisk indicate the best fit position of the distortion center at ROTATOR_REAL_ANGLE=0.0. (The direction of the ROTATOR_REAL_ANGLE is different from the OFFSET_ANGLE.)

4 Measuring the center of the distortion pattern (2)

The movement of the distortion pattern is further examined with the sky-camera mapping. In order to reduce the error caused by the tracking error etc, we only observed 10 stars at the edge of the field of view with a few stars at the center on the nights of 20080617. The results are summarized in Figure 4. As we expect, the radius of the circle of the distortion pattern movement changes as we change the position of the CMM. The radius of the circle and the center of the distortion pattern at ROTATOR_REAL_ANGLE=0deg is determined by fitting circle to the data points. The center of the circle is fixed at the measured rotator axis. The resulting best fit circles are shown in the figure. The residual of the fitting is 514 μm rms. for the (4700, -4200) dataset taken on 20080617.

The center of the distortion pattern at ROTATOR_REAL_ANGLE=0.0degree is summarized in Table 4. The conversions between the centers and the CMM positions are determined assuming coordinate conversion with rotation. The conversion is,

$$\begin{aligned}
 \text{DISTCEN_FPIX}_0 &= A \times \text{CMMX}(\mu\text{m}) + B \times \text{CMMY}(\mu\text{m}) + C, \\
 \text{DISTCEN_FPIY}_0 &= D \times \text{CMMX}(\mu\text{m}) + E \times \text{CMMY}(\mu\text{m}) + F \\
 A &= 0.987 \\
 B &= 0.162 \\
 C &= -1228.6 \\
 D &= -0.162 \\
 E &= 0.987
 \end{aligned}$$

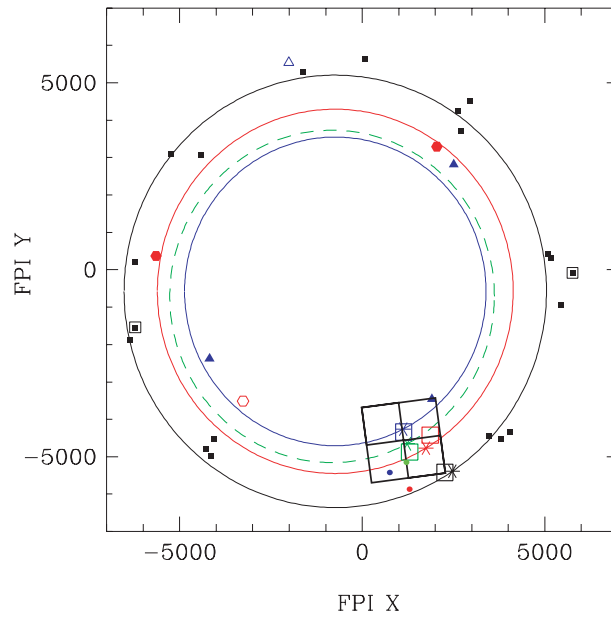


Figure 4: The measured positions of the distortion pattern center on the FPI coordinate from 200805 (only two points marked with filled square with large open square) and 200806 engineering observations. 200806 results shown with filled symbols are used for determine the best fit circle. Black, blue, and red symbols represents results with CMM at (4700,-4200), (3200,-4000), and (3700, -4500). The asterisk indicate the best fit position of the distortion center at ROTATOR_REAL_ANGLE=0.0. The results of 200801 (shown in the previous figure) are shown with green symbols.

	CMM position	Dist.Shift.Rot0	Fitted Dist.Shift.Rot0	
20080125	(3700, -3800)*	(1230, -4652)	(1807, -4540)	
Echidna reinstall				
20080617	(4700, -4200)*	(2465, -5390)	(2730, -5097)	
20080617	(3200, -4000)	(1121, -4260)	(1282, -4657)	
20080617	(3700, -4500)	(1743, -4769)	(1694, -5231)	
Echidna reinstall				
20080815	(3700, -4500)	(1404, -5784)	(1694, -5231)	
20080815	(3700, -4200)*	(1658, -5384)	(1743, -4935)	
20080815	(4700, -4200)	(3392, -4970)	(2730, -5097)	
20080815	(3700, -3200)	(2196, -3868)	(1905, -3948)	
20080816	(3700, -4200)	(1776, -4518)	(1743, -4935)	
20080816	(3700, -3200)	(1864, -3680)	(1904, -3948)	
20080816	(2700, -4200)	(1141, -5115)	(756, -4773)	
20080910	(3800, -4600)*	(1682, -5672)	(1776, -5347)	current value

Table 4: The best-fit distortion pattern center at ROTATOR_REAL_ANGLE=0.0 compared with the CMM positions. Fitted Dist.Shift.Rot0 shows Dist.Shift.Rot0 determined with equation shown in Sect.4. These Dist.Shift.Rot0 values correspond to telescope.model parameters No.23 and No.24, **but signs are inverted**. All values are in μm . Best CMM positions for each observing run are marked with asterisk.

$$F = -191.3 \tag{2}$$

During the fitting, scale is fixed to be 1.00 and X and Y orthogonalities are assumed. The CMM coordinate is 9.3 degree rotated against the FPI coordinate. The rotation is roughly consistent with the mechanical measurements of the CMM and FPI systems as shown in Appendix. The rms of the fitting is $346\mu\text{m}$ and $369\mu\text{m}$ in FPIX and FPIY coordinates. The origin of the CMM is at $(-1403, -694)$ with 20080909 measurements on the FPI coordinate. This is roughly consistent with the measured offset between the CMM center and the rotator center at $(-699, -645)$ ($\sim 1\text{mm}$, $\sim 1\text{mm}$).

5 Temperature dependence of the distortion pattern parameters

Using the center of the distortion pattern as described above, we fit the sky-camera mapping results again in order to refine the distortion model parameters. At first the three distortion parameters (PAR1, PAR2, PAR3) are fitted simultaneously. The results are shown in Table 5. The relation between the three parameters are plotted in Figure 5. There is a clear correlation between PAR2 and PAR3. If we use the middle PAR2 and PAR3 values as fiducials and plot the distortion pattern difference with the extreme values of PAR2 and PAR3 (and corresponding PAR1) from the fiducial pattern, the difference patterns are shown in the bottom panel. The difference is $0.1''$ at most at around 12 arcmin from the center.

In Figure 6, the dependence of the distortion parameters on the focus position (FAM values) are shown. PAR1 shows clear dependence on the FAM value, i.e. focal plane scale depends

Date	FieldID	PA(OFF)	FAM	T	PAR1(θ)	PAR2(θ^3)	PAR3(θ^5)	PAR4(θ/λ)	rms($''$)	Note
Design Required	value accuracy				0.291950 0.000032	0.0445 0.000540	0.0364 0.00842	-0.197		
20080514	field5	0(52)			0.290502	0.046430	0.001194	-0.197F	0.16	
20080514	field6	180(-118.1)			0.290600	0.042003	0.049526	-0.197F	0.19	
20080514	field9	0(71.2)			0.290475	0.051681	0.001150	-0.197F	0.16	
20080617	field50	90(108.1)			0.290580	0.042683	0.049064	-0.197F	0.17	
20080814	field21	0(103)	5.30		0.290569	0.042719	0.034522	-0.197F	0.20	
20080814	field30	0(-81)	5.05		0.290570	0.043843	0.012562	-0.197F	0.17	
20080814	field31	0(-82)	5.05		0.290536	0.046507	-0.017435	-0.197F	0.17	
20080814	field32	180(97)	5.05		0.290572	0.044360	0.032638	-0.197F	0.18	
20080814	field33	180(97)	5.05		0.290477	0.048028	-0.025634	-0.197F	0.18	
20080814	field50	0(-97)	5.30		0.290670	0.038582	0.073852	-0.197F	0.22	
20080814	field54	0(92)	5.25		0.290603	0.039828	0.080988	-0.197F	0.21	
20080909	field01	0(-95)	4.25	5.2	0.290628	0.044259	0.016995	-0.197F	0.16	
20080909	field02	180(85)	4.25	5.3	0.290646	0.042518	0.040994	-0.197F	0.17	
20080909	field03	180(75)	4.33	5.4	0.290657	0.041323	0.056532	-0.197F	0.18	
20080909	field04	0(90)	4.18	5.8	0.290624	0.044024	0.023733	-0.197F	0.15	
20080909	field09	0(-92)	4.20	5.9	0.290642	0.044004	0.020602	-0.197F	0.20	
20080909	field13	0(-92)	4.41	5.6	0.290625	0.043432	0.036534	-0.197F	0.18	bad seeing
20080909	field14	180(90)	4.41	5.6	0.290601	0.043425	0.035257	-0.197F	0.23	bad seeing
20081010	field01	0(-121)	5.10	1.8	0.290517	0.044998	0.015015	-0.197F	0.23	
20081010	field02	0(-42)	5.20	1.5	0.290547	0.044062	0.014459	-0.197F	0.19	
20081010	field12	0(65)	5.10	1.6	0.290551	0.044275	0.024467	-0.197F	0.23	
20081010	field13	90(158)	5.10	1.8	0.290514	0.047234	-0.021321	-0.197F	0.25	

Table 5: The distortion model parameters determined for each field. T represent truss temperature. Distortion parameter change which will make $0.1''$ difference at the edge of FoV shown as “Required accuracy”. “rms” represents rms residual after the fitting. PAR1 values are corrected by $+0.000041$ from the original measured values, based on wavelength dependence analysis. PAR1 is in (m/deg), PAR2 is in (m^3/deg^3), PAR3 is in (m^5/deg^5) and PAR4 is in (m/deg/nm).

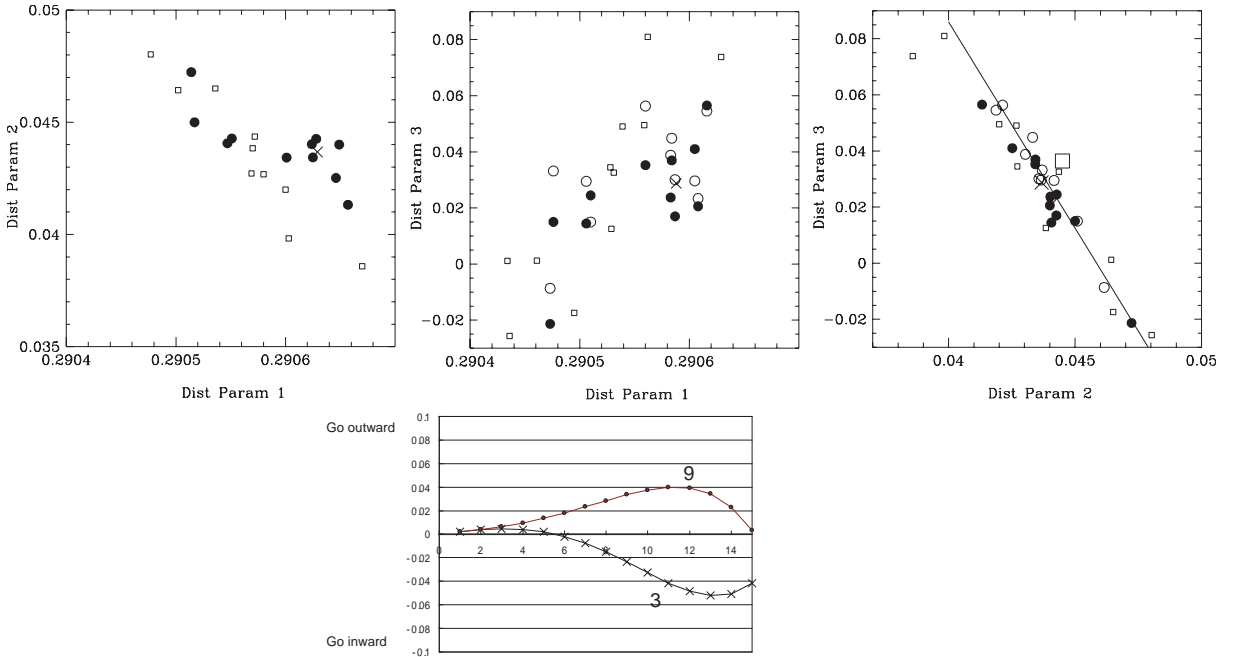


Figure 5: Relations between the distortion parameters. Black circle (small open square) represent results after (before) FAM tilt adjustment. Those values are from Table 5. Open circle represent values determined by fitting with PAR1 fixed with the relation shown in Figure 7. Those values are from Table 6. There is a good relation between PAR2 and PAR3. If we use the values from Table 6, the relation is fitted with $\text{PAR3} = 0.67408 - 14.702 \times \text{PAR2}$.

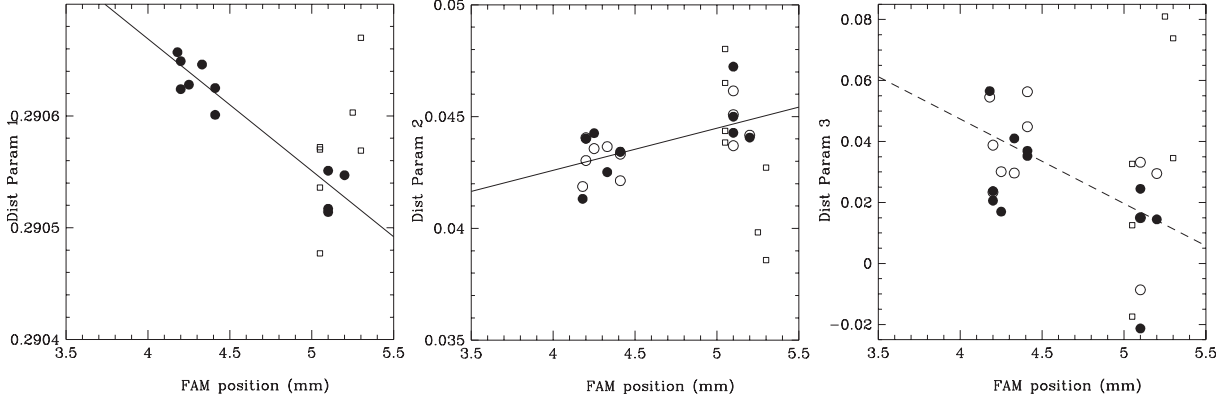


Figure 6: The dependence of the best fit distortion parameters to the FAM positions. The data taken after (before) the FAM tilt adjustment are plotted with filled circles (open squares). The FAM positions after the tilt adjustments are determined to best focus at center + 0.1mm. (Before the adjustment, best focus at center was used basically.) The scale parameter (distortion parameter 1) depends on the FAM position. The fitting results shown with solid lines (PAR1 = $0.291121 - 0.000115 \times \text{FAMvalue}$ and PAR2 = $0.03508 + 0.00188 \times \text{FAMvalue}$) The dotted line in the PAR3 figure shows the relation between PAR3 and FAM determined from PAR2-FAM and PAR2-PAR3 relations (PAR3 = $0.15833 - 0.02764 \times \text{FAM}$).

on the focus position. This is because when telescope tubing length is changed, the distance between the primary and the corrector is changed (the corrector z-direction is fixed to the telescope) and the off focus is corrected by only moving the instrument focus (thus, this is not the non-telecentricity, for non-telecentricity see Figure 10).

Then, we re-fit the distortion pattern with the PAR1 fixed to the values expected from the FAM value used in the observation. The results are shown in Table 6 and Figures 5 and 6 with open circles. Using the values, we fit the PAR2 dependence on the FAM value and the relation between PAR2 and PAR3. The results are shown in Figure 5 and 6 with solid lines. If we use these two relations, the PAR3 dependence on the FAM value can be determined. The relation is shown in the left panel of Figure 6 with dashed line. In summary, the dependence of PAR1, PAR2, PAR3 on the FAM value is

$$\begin{aligned}
 \text{PAR1} &= 0.291121 - 0.000115 \times \text{FAM}(\text{mm}) \\
 \text{PAR2} &= 0.03508 + 0.00188 \times \text{FAM}(\text{mm}) \\
 \text{PAR3} &= 0.15833 - 0.02764 \times \text{FAM}(\text{mm})
 \end{aligned}
 \tag{3}$$

The FAM value vary with the telescope-truss temperature as shown in Figure 7. If we use the FAM - truss temperature relation, the PAR1, PAR2, PAR3 dependence on the FAM values are converted to the dependence on the truss temperature. The results are,

$$\begin{aligned}
 \text{PAR1} &= (\text{No.10}) - (\text{No.20}) \times T(\text{C}) = 0.290500 + 0.00002363 \times T(\text{C}) \\
 \text{PAR2} &= (\text{No.11}) - (\text{No.21}) \times T(\text{C}) = 0.045225 - 0.00038634 \times T(\text{C}) \\
 \text{PAR3} &= (\text{No.12}) - (\text{No.22}) \times T(\text{C}) = 0.009176 + 0.005680 \times T(\text{C})
 \end{aligned}$$

Date	FieldID	PAR2(θ^3)	PAR3(θ^5)	rms($''$)	Note
20080909	field01	0.043570	0.030108	0.16	
20080909	field02	0.043658	0.029652	0.18	
20080909	field03	0.041875	0.054548	0.18	
20080909	field04	0.043036	0.038805	0.14	
20080909	field09	0.044057	0.023382	0.19	
20080909	field13	0.043322	0.044858	0.18	bad seeing
20080909	field14	0.042135	0.056318	0.23	bad seeing
20081010	field01	0.043701	0.033188	0.23	
20081010	field02	0.044170	0.029493	0.19	
20081010	field12	0.045091	0.014992	0.23	
20081010	field13	0.046152	-0.00864	0.25	

Table 6: The distortion model PAR2 and PAR3 determined with the PAR1 determined with the PAR1-FAM relation.

(4)

These relations are described in the telescope model using parameters, No.10, No.11, No.12 and No.20, No.21, No.22 as shown above. (It should be noted No.20 \times T, No.21 \times T, No.22 \times T are in the negative sign.) Using the ZEMAX model of the corrector, the expected temperature dependence of PAR1 is $+2.9 \times 10^{-5}$ (m/deg/K). The observed value is consistent with the expectation. The model does not show dependences of PAR2 and PAR3 on temperature, i.e. only scale changes in the model.

Using the PAR1,PAR2,PAR3 values expected from the outside temperature, the rms residuals of the sky-camera mapping are 0.17'',0.17'',0.18'',0.15'',0.21'' for 20080909-field01, 20080909-field02, 20080909-field03, 20080909-field04 and 20080909-field09, respectively.

6 Wavelength dependence of the distortion pattern

The dependence of the distortion pattern (focal plane scale) on the wavelength is described with the PAR4 of the distortion pattern parameter (No.13 of the telescope.model) as $PAR1 + PAR4/\lambda(nm)$. We examined the wavelength dependence with the spectroscopic rastering data taken in the low-resolution mode which covers entire wavelength range. The result is shown in Figure 8 with filled squares and crosses. The results are consistent with the PAR4 value determined with the ray-trace modeling shown with the solid line. The focal plane scale determined with the sky-camera mappings are shown with open squares. There is uncertainty in the effective wavelength of the sky-camera sensitivity. If we assume that the sky-camera effective wavelength is 700nm, then the measured scales are also consistent with the solid line. (AG-camera effective wavelength is estimated to be 760nm, but the CCD is different from the sky-camera).

7 Pointing center

Currently, the rotator axis is referred as the pointing center of the telescope, but the rotator axis does not match the origin of the FPI coordinate as described in Section 2. The configuration of the fiber is calculated from the origin of the FPI coordinate, and the RA-DEC coordinate of the origin need to be supplied to the fiber configuration software. The difference between

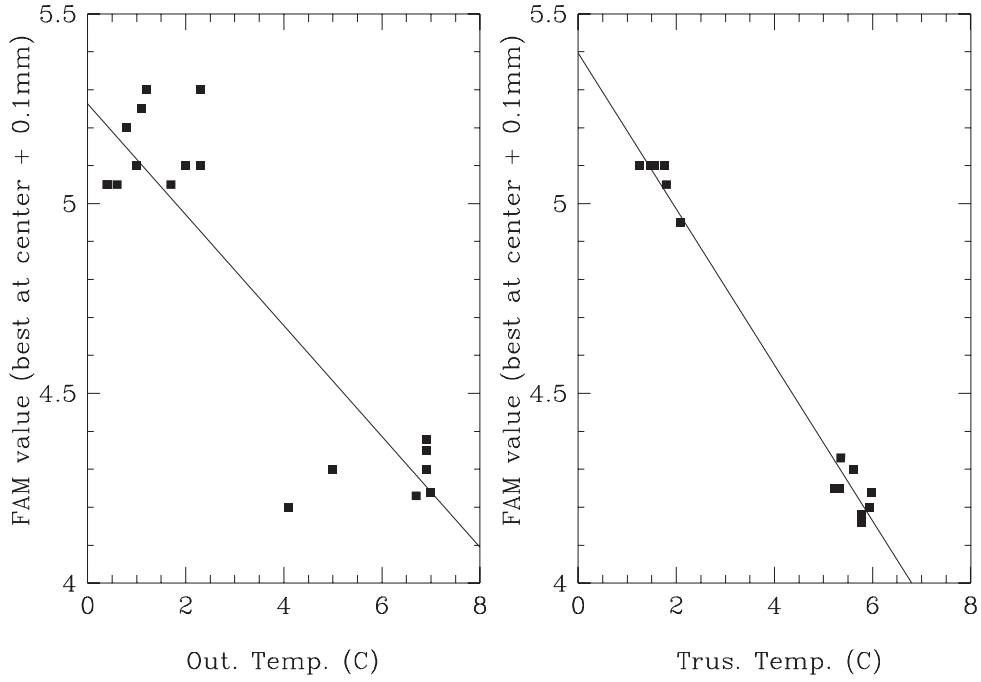


Figure 7: Left) The relation between the outside temperature and the best FAM position. The relation is fitted with $FAM = -0.146T + 5.263$. Right) Same for the truss temperature. The relation is $FAM(\text{mm}) = -0.2055 \times T(\text{C}) + 5.3963$. The dependence of the FAM value on the truss temperature is consistent with the ZEMAX model. The FAM value is correlated better with the truss temperature as expected.

Date	FieldID	1	2	3	4	Note
20081010	field15	0.16	0.16	0.16	0.15	NGC6633 PA=0
20081010	field16	0.17	0.16	0.15	0.15	NGC6633 PA=120
20081010	field22		0.17	0.16	0.16	M41 PA=0 large rotation

Table 7: The rms. residual of the sky-camera mapping using the final telescope model, columns 1 to 4 represent 1) after correcting mean offset, 2) correcting rotation, 3) fitting distortion parameters, and 4) fitting corrector distortion offset. There is no significant change even if we fit the distortion parameters, i.e. the parameters are determined well.

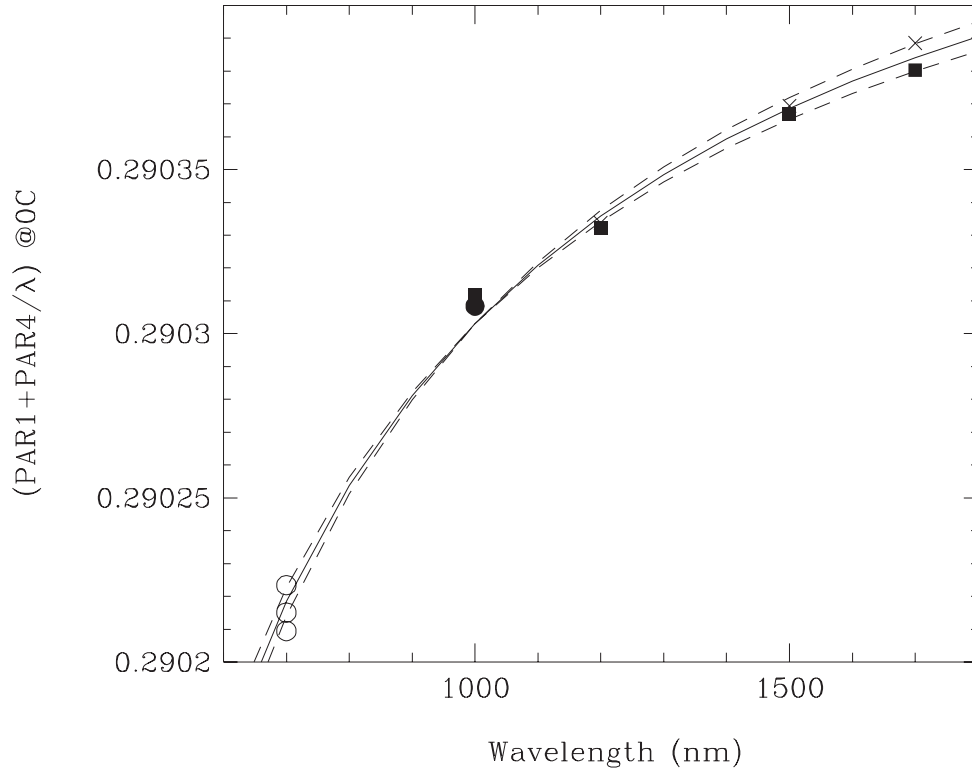


Figure 8: The dependence of the scale parameter $(PAR1+PAR4/\lambda(\text{nm}))$ on the wavelength. The measured scale parameters are corrected for temperature. The scale parameters measured with the spectroscopic rastering with Low-Resolution modes are shown with filled squares and crosses (200810 field20 and field21) and with J-Short mode is shown with filled circle (200810 field14). Those determined with the sky camera mappings are shown with open circles. The solid line shows the fiducial model which uses the PAR4 determined with the optical model (-0.197).

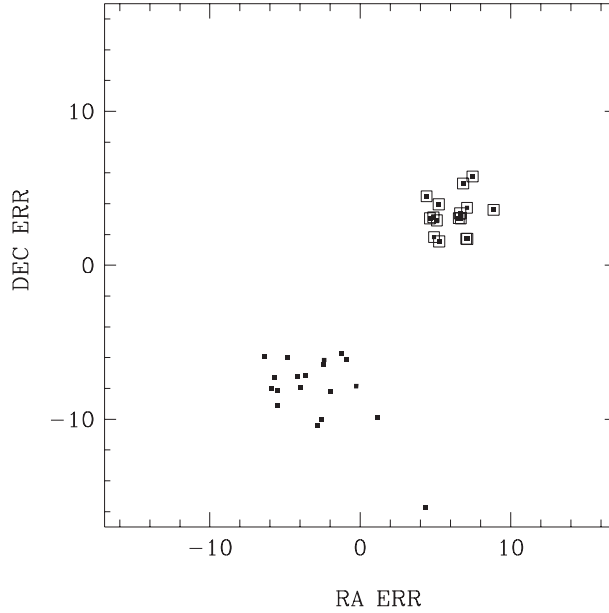


Figure 9: Measured pointing error for various field, the difference of the RA-DEC coordinate of the rotation center from the target RA-DEC coordinate. Data taken before meridian are marked with open squares.

the pointing center of the telescope and the origin of the FPI coordinate is handled with the environmental variables, POINTING_OFFSET_RA and POINTING_OFFSET_DEC.

We evaluate the pointing errors with the current telescope pointing model (determined by PA) by checking RA-DEC coordinate of the rotator axis with the sky-camera mapping data. The resulting offsets between the target coordinate and the RA-DEC coordinate of the rotator axis is shown in Figure 9. There is a large offset between the data points taken before and after meridian. Need to be checked..

8 Guide fiber focus positions

Memo: skycamera focus 4.7mm and AGSH focus 3.4mm. Center 4.9mm then edge 5.1mm-5.15mm. If sky-camera best focus at center is 5.15mm then, best focus for science fiber is 5.15mm, best focus for sky-camera mapping is 5.30mm, roughly.

9 Appendix: calibration items summary

IF WE RE-INSTALL PIR TO TELESCOPE, the coma-free CMM position can be changed. No.23 and No.24 telescope.model parameters need to be changed using the updated CMM position and the equation shown in Section 4. It should be noted that the equation may be changed if we re-install Echidna to PIR. (The radius of the circle of the distortion pattern movement can be changed).

IF WE RE-INSTALL ECHIDNA TO PIR, the position of the rotator axis on the FPI coordinate can be changed. We need to determine the rotator center on the FPI coordinate as

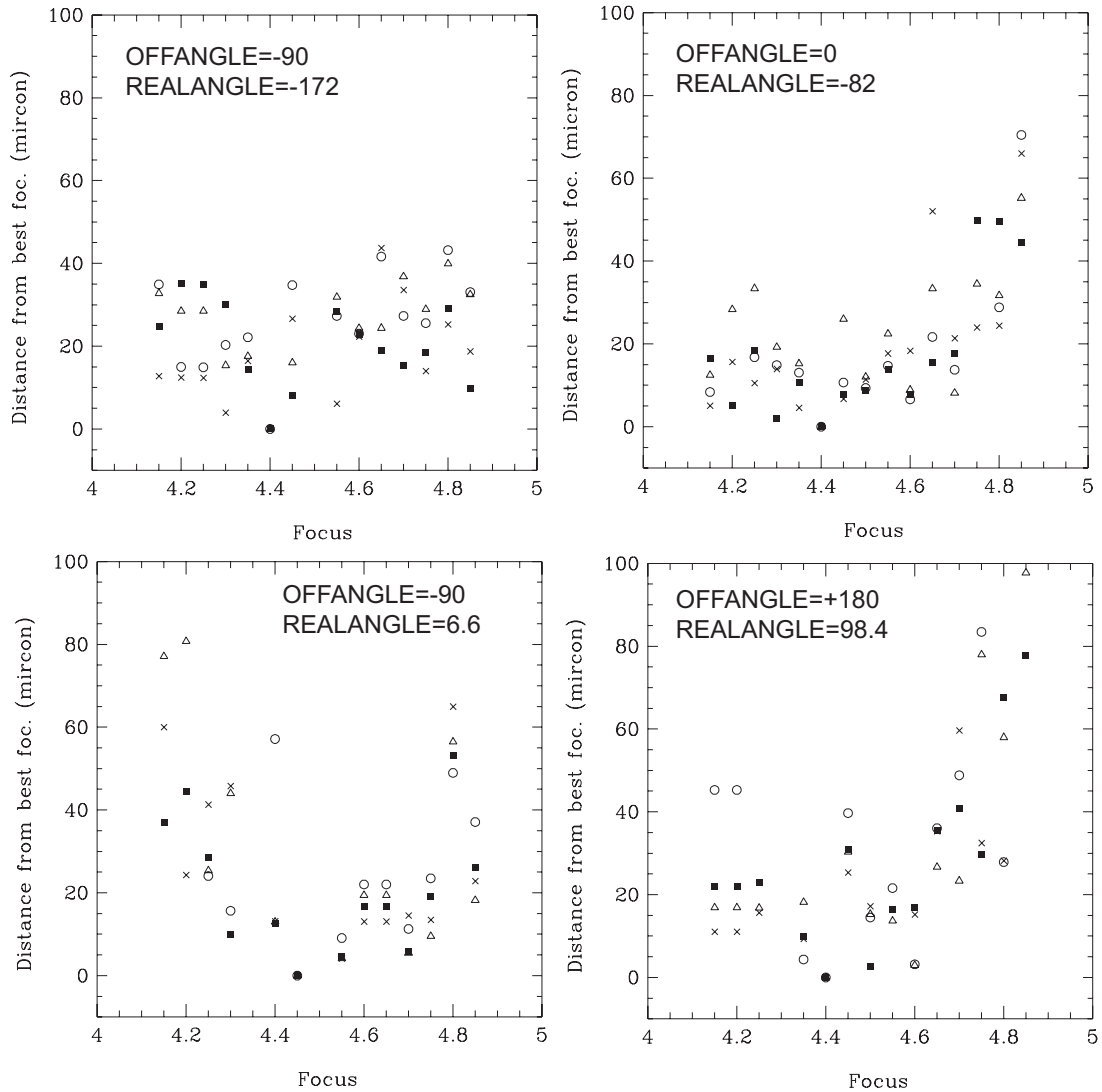


Figure 10: The effect of the offocus on the centroiding of the sky camera mapping. The position of four stars at the edge of the FoV are measured relative to the position of the star at the center. The movement of the relative positions are plotted as a function of FAM focus position (mm). The best focus position was around FAM=4.4(mm) and the position at this focus was used as the base position. Off focus by 0.2mm can affect the measured position of the stars by $20\mu\text{m}$ at most.

Parameter	Value	Note
SKYC_AKIYAMA_A	-8.041	see Sec.1. (20080814)
SKYC_AKIYAMA_B	0.203	see Sec.1. (20080814)
SKYC_AKIYAMA_C	3575.0	see Sec.1. (20080814)
SKYC_AKIYAMA_D	-0.195	see Sec.1. (20080814)
SKYC_AKIYAMA_E	-8.364	see Sec.1. (20080814)
SKYC_AKIYAMA_F	2610.0	see Sec.1. (20080814)
SKYC_CENTRE_X_OFFSET	600	Set to be stars can be caught at center.
SKYC_CENTRE_Y_OFFSET	70	Set to be stars can be caught at center.
ROTATOR_AXIS_X	456	see Sec.2 Tab.2. sign is inverted by definition (20081011)
ROTATOR_AXIS_Y	521	see Sec.2 Tab.2. sign is inverted by definition (20081011)
POINTING_OFFSET_RA	-9.12	At PA=0, for FPI(0,0), this needs to be subtracted from commanded RA
POINTING_OFFSET_DEC	+7.20	Depending on ROTATOR_AXIS_X At PA=0, for FPI(0,0), this needs to be subtracted from commanded DEC Depending on ROTATOR_AXIS_Y
telescope.model No.10	0.290500	see Sec.5. (20081011)
telescope.model No.11	0.045225	see Sec.5. (20081011)
telescope.model No.12	0.0091763	see Sec.5. (20081011)
telescope.model No.13	-0.197	see Sec.6. (20081011)
telescope.model No.20	-0.00002363	No.10 parameter dependence on temperature. (20081011)
telescope.model No.21	0.0003863	No.11 parameter dependence on temperature. (20081011)
telescope.model No.22	-0.005680	No.12 parameter dependence on temperature. (20081011)
telescope.model No.23	-1776	depends on CMM position , see Sec.4,Tab.5, sign is inverted from Tab.4, Fig.4 by definition
telescope.model No.24	5347	depends on CMM position , see Sec.4,Tab.5, sign is inverted from Tab.4, Fig.4 by definition
telescope.model No.25	Not used	echTelMdl.cc revised such that No.23,24 refer to ROTATOR_REAL_ANGLE=0deg
telescope.model No.26	Not used	echTelMdl.cc revised such that No.23,24 refer to ROTATOR_REAL_ANGLE=0deg
telescope.model No.27	Not used	echTelMdl.cc revised such that No.23,24 refer to ROTATOR_REAL_ANGLE=0deg
telescope.model No.28	Not used	echTelMdl.cc revised such that No.23,24 refer to ROTATOR_REAL_ANGLE=0deg

Table 8: Summary of the best estimate environmental variables for ICS and telescope model parameters related to the distortion pattern modeling. It should be noted that POINTING_ERR does not relate to the pointing error of the telescope, relate to the offset between the rotator axis and the FPI origin. These values are described in \$ECONFIG/.zshrc and \$ECONFIG/telescope.model. The definitions of the parameters No.10, No.11, No.12, No.20, No.21, No.22, No.25, No.26, No.27 are changed from the original modeling.

described in Section 2 and Table 2. ROTATOR_AXIS_X and ROTATOR_AXIS_Y, and POINTING_ERR_RA and POINTING_ERR_DEC environmental variables need to be updated.

The relation between the CMM coordinate and the FPI coordinate can be changed (parameters shown in Section 4). The shift of the relation can be checked by measuring the center of the distortion pattern at ROTATOR_REAL_ANGLE=0.0. If the center is measured at ROTATOR_REAL_ANGLE=0.0 additionally, the matching between the rotator axis and the center of the circle of the distortion pattern movement can be checked.

IF WE RE-INSTALL SKY-CAMERA, then we need to determine the relation between SKY-camera coordinate and FPI coordinate as described in Section 1 and Table1. SKYC-environmental variables need to be updated.

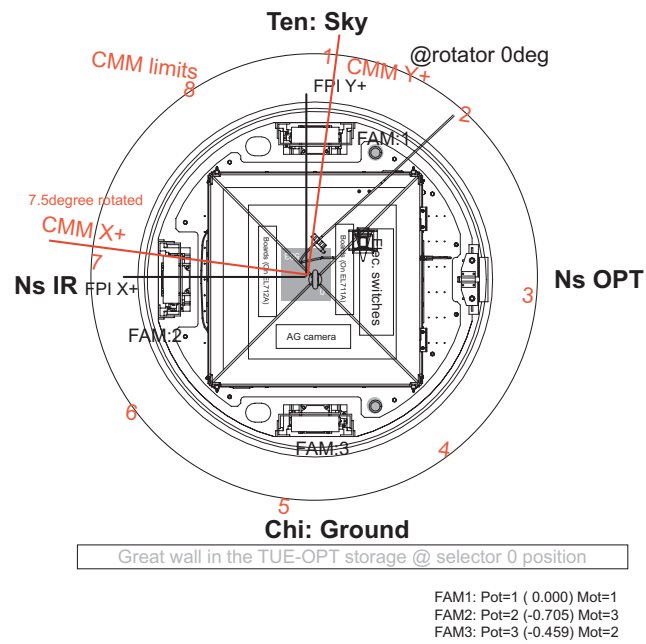


Figure 11: The relation between the Echidna unit and the PIR/CMM unit at rotator angle of 0 degree. CMM axis is 7.5 degree rotated against Echidna coordinate (measurements by M.Kimura)